Available online at www.sciencedirect.com
ScienceDirect
Optical Materials xxx (2006) xxx–xxx
OPTICAL Materials
www.elsevier.com/locate/optmat

Dopant segregations in oxide single-crystal fibers grown by the micro-pulling-down method

Dirk Maier [a,*], Dieter Rhede [b], Rainer Bertram [a], Detlef Klimm [a], Roberto Fornari [a]

[a] Institute for Crystal Growth, Max-Born-Strasse 2, 12489 Berlin, Germany
[b] Geoforschungszentrum Potsdam, Telefgrafenberg, 14473 Potsdam, Germany

Abstract

$(Cr, Al)_2O_3$ ($k_0 = 2$), $(Ga, Al)_2O_3$ ($k_0 = 0.3$), $Gd_3(Cr, Ga)_5O_{12}$ ($k_0 > 1$), $(Gd, Yb)_3Ga_5O_{12}$ ($k_0 > 1$) and $(Yb, Y)_3Al_5O_{12}$ ($k_0 > 1$) fibers have been grown by the micro-pulling-down method. k_0 is the equilibrium distribution coefficient of the dopant with respect to the given host phase. The axial and radial dopant distribution was measured by electron probe microanalysis. The growth interface was frozen by pulling-down the fiber rapidly and quenching the molten zone. In the case of growth with a thin melt zone of about 30–70 μm between growth front and crucible nozzle radial dopant distributions in form of a homogeneous core and a peripheral rim of different composition were found in all fibers. The growth interface has a bump into the crucible nozzle. For $(Yb, Y)_3Al_5O_{12}$, $Gd_3(Cr, Ga)_5O_{12}$, $(Gd, Yb)_3Ga_5O_{12}$ and $(Ga, Al)_2O_3$ mainly diffusional transport in the crucible nozzle was found. The dopant concentration is higher or lower at the rim than in the core for $k_0 < 1$ or $k_0 > 1$, respectively. This axial segregation corresponds to the bend interface. In the case of $(Cr, Al)_2O_3$ convective transport inside the crucible nozzle was found. Also, different to the diffusive case, the Cr_2O_3 concentration in the rim is higher than in the core region although $k_0 > 1$. The growth with a higher melt zone of about 200 μm has the same axial segregation behaviour but the radial segregation is strongly suppressed. The interface is spherical. The experiments show, that the radial and axial concentration profiles that are the result from the micro-pulling-down growth of solid solutions are influenced by the distribution coefficient, the geometry of the crucible, the height of the molten zone and melt properties.

PACS: 81.10.−h; 81.10.Fq; 81.70.Jb

Keywords: Single crystalline fiber; Dopant profiling; Oxides; Micro-pulling-down

1. Introduction

Since the development of the micro-pulling-down method by Fukuda [1] different types of oxide fibers have been grown. Uda found radial Mn segregations for $Mn:LiNbO_3$ which was explained by assuming an interfacial electrical field acting on the different charged ions [2]. Ganschow also reported strong radial segregations in the case of olivine fiber growth, which is a solid solution of fayalite and forsterite [3]. This radial segregation leads to an inner interface between a core and a rim region of different composition. Therefore, for optical fibers a refractive index change is to be expected [4,5].

The aim of this work is to find a general explanation of the segregation behaviour of oxide fibers grown by the micro-pulling-down method.

2. Experimental

In Table 1 we show a list of the crystals studied in this work. The corresponding starting materials were prepared from 4 N Al_2O_3, Cr_2O_3, Ga_2O_3, Gd_2O_3, Y_2O_3 and Yb_2O_3 powders by grinding a total weight of 5 g in a plastic mortar, pressing into pellets and sintering at 2/3 of the melting temperature in platinum–gold crucibles.

* Corresponding author. Tel.: +49 30 6392 2827; fax: +49 30 6392 2803.
E-mail address: maier@ikz-berlin.de (D. Maier).

0925-3467/$ - see front matter © 2006 Elsevier B.V. All rights reserved.
doi:10.1016/j.optmat.2006.10.023

Table 1
Melt compositions and the corresponding equilibrium distribution coefficient, growth rates and growth types used in this work

Abbreviation	Chemical formula/dopant concentration (mol%)	Growth rates (mm/min)/growth type	k_0
Cr:Al_2O_3	(Cr, Al)$_2O_3$ 1.75% Cr_2O_3	0.5/1, 2	2 [8]
Ga:Al_2O_3	(Ga, Al)$_2O_3$ 1.5% Ga_2O_3	0.3/1, 2	0.3 [8]
Cr:GGG	$Gd_{3.05}(Cr, Ga)_{4.95}O_{12}$ 1.75% Cr_2O_3	0.3/1	≈3
Yb:GGG	$(Yb, Gd)_{3.05}Ga_{4.95}O_{12}$ 5% Yb_2O_3	0.3/1	>1
Yb:YAG	$(Yb, Y)_3Al_5O_{12}$ 5.7% Yb_2O_3	0.3/1	>1

The oxide fibers were grown using a micro-pulling-down apparatus with induction heating. A 5 ml iridium crucible with 500 mg of the starting material was placed on an iridium after-heater and heated by the inductor coil of a 10 kW rf Generator. The crucible after-heater arrangement was surrounded by a zirconia fiber tube and a high-purity alumina tube for thermal insulation. The experiments were carried out in a vacuum-tight steel chamber, 35 l in Volume. It was evacuated before each experiment to 5×10^{-3} mbar and filled with 5 N N_2 Gas for Cr:Al_2O_3 and Yb:YAG. To suppress the reduction of Ga_2O_3 to the volatile Ga_2O 50% CO_2 in the case of Ga:Al_2O_3, Cr:GGG and Yb:GGG was added to the N_2. During growth a constant flow of about 900 ml/min was kept. The axial temperature gradient was estimated to be about 500 K/cm by seeding with a W5Re/W26Re thermocouple and measuring the temperature during pulling every 0.5 mm. To get the dopant distributions described in this paper it was important to have a flat polished crucible nozzle. During growth the height of the molten zone was carefully controlled by manually increasing or decreasing the rf-power. Two growth arrangements with different heights of the molten zone have been selected by adjusting the rf-power. Type 1 with only a melt film of about 30–70 μm between crucible nozzle and crystal and a crystal diameter equal to the capillary outer diameter. Type 2 with a considerable meniscus of about 200 μm height and a crystal diameter of about 85% of the capillary outer diameter (Fig. 2). Radial and axial cross-sections of the grown fibers have been prepared and concentration profiles were determined by electron probe microanalysis (EPMA).

3. Results and discussion

The maximum growth velocity for the micro-pulling-down growth was estimated by Tillers criterion. At velocities higher than the estimated maximum growth rate, constitutional undercooling will result in cellular structures and inclusions.

As it can be seen in Fig. 1 the type 1 fibers are constant in diameter and have a smooth surface. This is mainly controlled by the very stable melt film in growth type 1, even in the case of the strongly wetting and creeping Cr:GGG melt. Type 2 fibers have a rough surface due to a less stable molten zone. The growth of Cr:GGG with type 2 is not possible because of strong creeping melt in this case.

Except in the case of Cr:Al_2O_3 all fibers have constant axial concentration, which was confirmed by induction coupled plasma optical emission spectroscopy (ICP-OES) at three equidistant pieces of the fibers (Table 2). The advantage of the ICP-OES method compared to EPMA (electron probe microanalysis) is that one has the average composition over the full volume of the fiber pieces. With EPMA it is difficult to map the axial segregation profile because of the strong radial inhomogeneity and the limited size of the electron beam. This constant axial concentration suggests a fully diffusive transport regime in the crucible nozzle. Due to relative high pulling rate and no mixing in the capillary the diffusion length $\beta = D/v$ (v: growth rate, D: diffusion rate) is smaller than the inner length of the crucible capillary (3.5 mm). Therefore we get an effective distribution coefficient equal to one.

In the case of Cr:Al_2O_3 the Cr_2O_3 concentration drops in the growth direction which indicates a thin diffusion boundary layer at the growth interface and convective melt mixing in melt container and the crucible capillary. The mean interface concentration profile can be fitted well by the macrosegregation theory of Favier [6], which describes the transient axial segregation during unidirectional solidification at constant rate. This leads to an effective distribution coefficient of $k_{\text{eff}} \approx 1.3$ (Fig. 5a,b). This convection is believed due to a thermo-solutal effect. The dopant depleted melt at the growth interface ($k_0 > 1$) is less dense than the melt in the container, so this concentration gradient could act as a driving force for convections in the low viscosity Al_2O_3 melt inside the capillary. Numerically simulations for this effect are in progress.

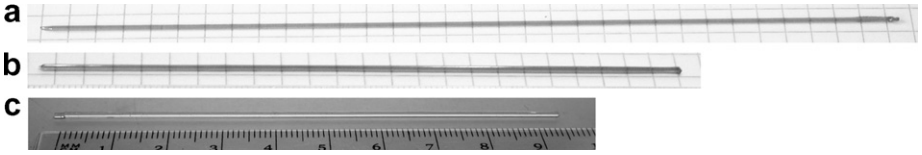

Fig. 1. Photographs of some selected type 1 fibers (a) Cr:GGG; (b) Cr:Al_2O_3 and (c) Yb:YAG.

Please cite this article in press as: D. Maier et al., Opt. Mater. (2006), doi:10.1016/j.optmat.2006.10.023

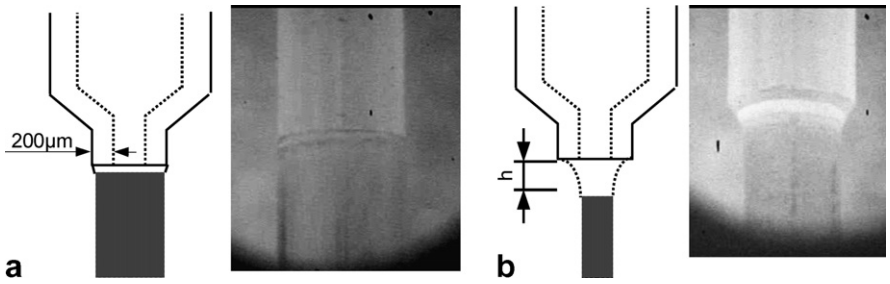

Fig. 2. (a) Growth type 1 with only a melt film between crucible nozzle and fiber and (b) growth type 2 with a considerable meniscus.

Table 2
Axial concentrations in mol% measured by ICP-OES

Fiberpart	$Ga:Al_2O_3$	Yb:YAG	Yb:GGG	Cr:GGG
Begin	1.00	5.70	5.15	1.71
Middle	1.12	5.67	5.14	1.85
End	1.03	5.69	5.13	1.8
Initial	1.5	5.65	5.0	1.75

All type 1 fibers show strong radial segregations (Figs. 4 and 5c). The fibers grown in the pure diffusive regime have a lower or higher dopant concentration in the rim region than the core region for $k_0 > 1$ or $k_0 < 1$, respectively. This can be explained by the form of the growth interface.

Fig. 3 shows a axial cross-section backscattered electron image (BSE) of a quenched fiber end. The contrast in BSE images is sensitive to the chemical composition. For comparison of BSE image contrast to the dopant concentration in Fig. 3 an EDX (energy dispersive X-ray spectroscopy)-linescan is overlapped. So one can clearly see the growth interface and the surrounding quenched melt (sketched by a dashed line). The growth interface is convex towards the melt. The bump in the interface is shaped by the diameter of the capillary outlet. During growth the radial movement of the fiber was blocked by the capillary wall, which shows that the bump reaches into the capillary. Therefore, the radial distribution in the fully diffusive range and for a small diffusion length β, which is the case in micro-pulling-down growth of oxides, can be explained by the solution of the diffusion equation by singular perturbation theory with a curved growth front as boundary condition [7]. Two theoretical curves calculated by this theory for a cosine shaped interface, which could be used as a simplification, and $k_0 < 1$ and $k_0 > 1$ are shown in Fig. 6. The equilibrium distribution coefficient and the growth rate were taken similar

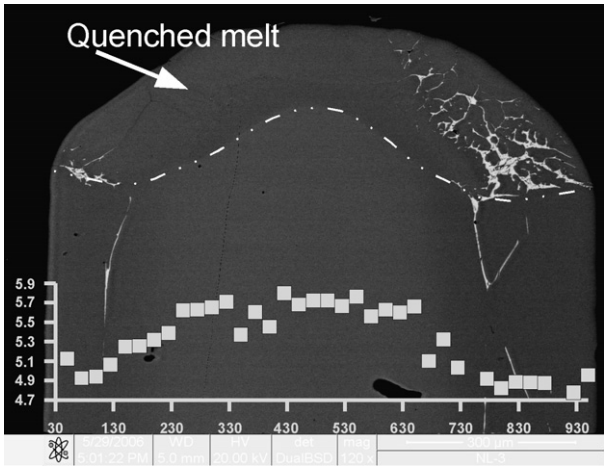

Fig. 3. BSE image of a quenched molten zone of a Yb:YAG fiber. The form of the growth interface (marked by a dashed line) can be seen by the lower chemical contrast of the dopant depleted melt and cracks due to rapid moving and quenching of the melt. To interpret the image contrast a EDX linescan of Yb_2O_3 is overlapped.

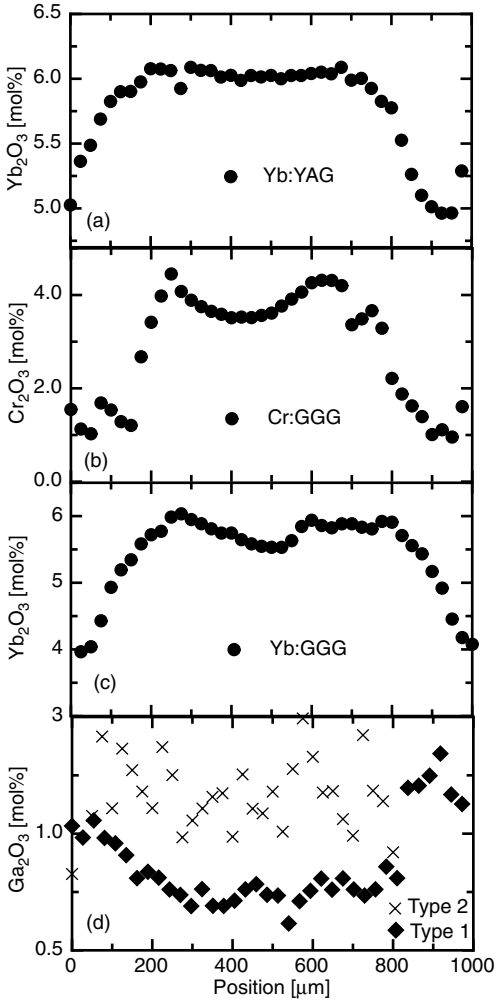

Fig. 4. Radial concentration profiles of type 1 (a) Yb:YAG; (b) Cr:GGG; (c) Yb:GGG; (d) type 1 and type 2 $Ga:Al_2O_3$.

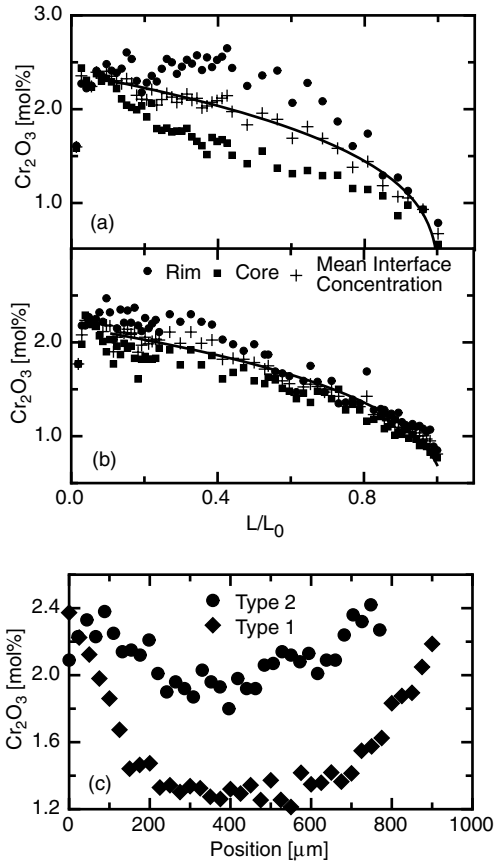

Fig. 5. (a) Axial concentration profile of type 1 Cr:Al_2O_3 and (b) axial concentration profile of type 2 Cr:Al_2O_3. The mean interface concentration is fitted by the macrosegregation theory of Favier [6], which gives a k_{eff} of 1.30 (type 1) and 1.27 (type2). (c) Radial concentration profiles of type 1 and type 2 Cr:Al_2O.

to the experiment and the diffusion rate in the range of 10^{-5} cm^2/s as it is common for oxide melts. Fitting was not possible because of a non-symmetric growth interface, but the theory depends on an interface with radial symmetry. However the results look very comparable.

In the case of Cr:Al_2O_3 the same interface shape is observed, but the radial Cr_2O_3 distribution (Fig. 5c) is not conform with the theory of Coriell. It shows a behaviour similar to a case of $k_0 < 1$, according to Coriell's theory, but the distribution coefficient of Cr_2O_3 is greater than one. So here it is believed, that this radial concentration profile is formed by convectional transport along the interface.

The type 2 fibers show the same axial segregation behaviour like the type 1 fibers but the radial concentration profile is flatter than the type 1 fibers and more irregular. During growth it is observed that the interface is slightly spherical and radial movement of the fiber during growth is possible. So we have less interface deflection and stronger Marangoni convection at the free melt/gas interface of the considerable meniscus and therefore a flatter radial dopant distribution. The irregularities in the type 2 Ga:Al_2O_3 are maybe due to strong Marangoni swirls caused by the melt/gas interface, which enrich the melt with dopant close to the growth interface.

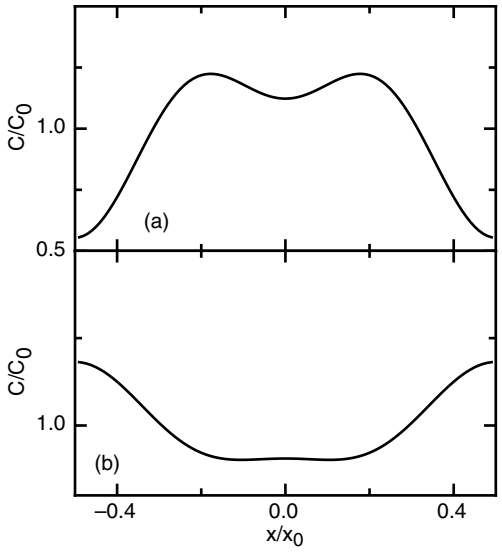

Fig. 6. Theoretical curves calculated by the theory of Coriell [7] for (a) $k = 3$, $v = 0.7$ mm/min, $D = 3 \times 0^{-5}$ cm^2/s and (b) k=0.3, $v = 0.3$ mm/min, $D = 5 \times 10^{-6}$ cm^2/s.

4. Conclusions

Cr:Al_2O_3, Ga:Al_2O3, Cr:GGG, Yb:GGG and Yb:YAG fibers have been grown by the micro-pulling down method. The growth with a thin melt zone of about 30–70 μm between growth front and crucible nozzle leads to radial dopant distributions modulated by the shape of the growth interface. The growth interface has a bump into the crucible nozzle. For Ga:Al_2O_3, Cr:GGG, Yb:GGG and Yb:YAG mainly diffusional transport in the crucible nozzle was found. In the diffusive case, the dopant concentration is higher or lower at the rim than in the core for $k_0 < 1$ or $k_0 > 1$, respectively. For Cr:Al_2O_3 convective transport inside the crucible nozzle was found. This could be attributed to a thermo-solutal effect caused by the lower density of the dopant depleted melt at the interface and the low viscosity of the Al_2O_3 melt. The growth with a higher melt zone of about 200 μm has the same axial segregation behaviour but the radial segregation is strongly suppressed due to Marangoni convection at the melt/gas boundaries. The interface is spherical. The experiments show, that the radial and axial concentration profiles are influenced by the distribution coefficient, the geometry of the crucible, the height of the molten zone and melt properties.

References

[1] N. Schäfer, Y. Yamada, K. Shimamura, H.J. Koh, T. Fukuda, J. Cryst. Growth 166 (1996) 675.
[2] S. Uda, J. Kon, K. Shimamura, J. Ichikawa, K. Inaba, T. Fukuda, J. Cryst. Growth 182 (1997) 403.
[3] S. Ganschow, D. Klimm, Cryst. Res. Technol. 40 (2005) 359.
[4] D. Pelenec et al., Opt. Comm. 115 (1995) 491.
[5] J.H. Sharp, R. Illingworth, S. Ruddock, Opt. Lett. 22 (1998) 109.
[6] J.J. Favier, Act. Met. 29 (1981) 197.
[7] S.R. Coriell, R.F. Boisvert, R.G. Rehm, J. Cryst. Growth 54 (1981) 167.
[8] ACerS-NIST Phase Equilibria Diagrams Database Version 3.0.1.

Please cite this article in press as: D. Maier et al., Opt. Mater. (2006), doi:10.1016/j.optmat.2006.10.023